รายงานฉบับสมบูรณ์

โครงการวิจัยร่วมภาครัฐและเอกชน
ระบบผลิตอัตโนมัติเพื่อการพัฒนาอุตสาหกรรมการผลิตขั้นสูง

เรื่อง

โครงการ A New Method for Continuum Mechanics Modeling for Design and Manufacturing

โดย

ผศ.ดร. กุณฑินี มณีรัตน์

ภาควิชาวิศวกรรมเครื่องกล
คณะวิศวกรรมศาสตร์ จุฬาลงกรณ์มหาวิทยาลัย

กรกฎาคม 2548

รายงานฉบับสมบูรณ์

โครงการวิจัยร่วมภาครัฐและเอกชน
ระบบผลิตอัตโนมัติเพื่อการพัฒนาอุตสาหกรรมการผลิตขั้นสูง

เรื่อง

โครงการ A New Method for Continuum Mechanics Modeling for Design and Manufacturing

โดย

ผศ.ดร. กุณฑินี มณีรัตน์

ภาควิชาวิศวกรรมเครื่องกล
คณะวิศวกรรมศาสตร์ จุฬาลงกรณ์มหาวิทยาลัย

กรกฎาคม 2548

โครงการ **A New Method for Continuum Mechanics Modeling for Design and Manufacturing**

โดยแบ่งตามหัวข้อวิจัยได้ดังนี้

การพัฒนาโปรแกรมคอมพิวเตอร์สำหรับการจำลองแบบกลศาสตร์ทางคณิตศาสตร์

จุดประสงค์ พัฒนาโปรแกรมคอมพิวเตอร์ที่ง่ายต่อการพัฒนาและใช้งาน

การดำเนินงาน
1. วางโครงสร้างโปรแกรม โดยใช้ภาษา C++ .ในลักษณะ Object Oriented โดยใช้ Tensor Operation เป็น Class พื้นฐานหลัก ซึ่งอยู่ในระหว่างการพัฒนาและ Verification
2. พัฒนาการจำลองแบบแบบ multiphysics ของของแข็งและความร้อน
3. พัฒนาปรับปรุงการวิเคราะห์ grid independency ในการจำลองแบบโดยใช้การสร้างกริดแบบ Delaunay Triangulation และการทำ Adaptive Grid

ผลลัพธ์
1. ได้นำเสนอผลงานในการประชุมทางวิชาการดังนี้

   Lertsurayut, T. and Maneeratana, K. 2002. The utilisation of delaunay triangulation in finite volume modelling, Proceedings of the 16th Conference of the Mechanical Engineering Network of Thailand (ME-NETT 16). Kata Beach Resort, Phuket, 14-16 October 2002, pp. 262-267.
2. เป็นหัวข้อวิทยานิพนธ์ปริญญามหาบัณฑิต โดยยังอยู่ในขั้นตอนการวิจัย

การพัฒนาการออกแบบโดยใช้การจำลองแบบกลศาสตร์ทางคณิตศาสตร์และขั้นตอนวิธีทางพันธุกรรม

จุดประสงค์ พัฒนาการออกแบบ topology ของโครงสร้างแบบวิวัฒนาการ

การดำเนินงาน
1. พัฒนาการออกแบบ topology โดยใช้ขั้นตอนวิธีทางพันธุกรรมและการจำลองแบบกลศาสตร์ทางคณิตศาสตร์โดยระเบียบวิธีไฟไนต์วอลุม
2. พัฒนาการออกแบบแบบ multi-objective และพัฒนา crossover operator .ในขั้นตอนวิธีทางพันธุกรรมสำหรับใช้งานเฉพาะด้าน

ผลลัพธ์
1. ได้นำเสนอผลงานในการประชุมทางวิชาการดังนี้

   Maneeratana, K. 2002. A feasibility study on the continuum topology design by genetic algorithm and finite volume method, Proceedings of the 16th Conference of the Mechanical Engineering Network of Thailand (ME-NETT 16). Kata Beach Resort, Phuket, 14-16 October 2002, pp. 256-261.

2. เป็นหัวข้อวิทยานิพนธ์ปริญญาดุษฎีบัณฑิต โดยยังอยู่ในขั้นตอนการวิจัย

การจำลองแบบเพื่อใช้ในอุตสาหกรรม: การจำลองแบบการแข็งตัวของน้ำแข็ง

จุดประสงค์		พัฒนาต้นแบบทางคณิตศาสตร์และโปรแกรมคอมพิวเตอร์เพื่อการจำลองแบบการแข็งตัวของน้ำแข็งสำหรับการพัฒนาประสิทธิภาพในอุตสาหกรรมน้ำแข็งซอง
การดำเนินงาน	1.	ศึกษาการจำลองแบบการเปลี่ยน phase และจำลองแบบเพื่อหา parameters ที่เหมาะสม
	2.	จำลองแบบการแข็งตัวของน้ำแข็งในซองน้ำแข็งจริง
ผลลัพธ์	1.	เป็นวิทยานิพนธ์ปริญญามหาบัณฑิต สาขาวิศวกรรมเครื่องกล ปีการศึกษา 2545 เรื่อง การจำลองแบบการขึ้นรูปของน้ำแข็งโดยระเบียบวิธีไฟไนต์วอลุม โดย นางสาวรจนา ประไพนพ
	2.	บทความทางวิชาการ โดยกำลังรอการตอบรับจากวารสารภายในประเทศ

การประชุมวิชาการเครือข่ายวิศวกรรมเครื่องกลแห่งประเทศไทยครั้งที่ 16
14 – 16 ตุลาคม 2545 จังหวัดภูเก็ต

A Feasibility Study on the Continuum Topology Design by Genetic Algorithm and Finite Volume Method

Kuntinee MANEERATANA
Department of Mechanical Engineering, Faculty of Engineering, Chulalongkorn University,
Phaya Thai Road, Pathum Wan, Bangkok 10330 Thailand
Phone 66(0)2218-6610 Fax 66(0)2252-2889 E-mail: kuntinee.m@chula.ac.th

Abstract

This paper presents a preliminary investigation on the use of the genetic algorithm (GA) and finite volume (FV) method in the topology design of structures such that desired 'performances' are optimised. First, the designing domain is divided into rectangular parallelepiped grids. By selective filling these grids with grid-shaped solid blocks or leaving the grid spaces empty, different structural patterns are obtained. Performances of structures are calculated by FV simulations and a basic GA procedure searches for optimum block arrangements. A 2D heat conduction problem with the spatial domain composed of a structured 4 × 3 grid is used as an example. The design objective is to obtain the configuration that can best dissipate heat into the surroundings. Results of the test run are promising. Two mirror-image optimum configurations are obtained within 19 generations, each generation involves 20 ad hoc chromosomes, compared with the entire combinatorics of 4096.

Keywords: Structural design optimisation, topology, genetic algorithm, finite volume method.

1. Introduction

At present, there are two main optimisation approaches, the derivative-based and derivative-free methods. The derivative-based schemes, such as Newton's and conjugate gradient (CG) methods, have long been used in structural design. On the other hand, the derivative-free optimisation, such as genetic algorithm (GA) and simulated annealing (SA), are much less employed in mechanical engineering applications, mostly confined to the field of control, machine intelligence and CAD/CAM.

Compared to the derivative-based schemes, the derivative-free methods do not need functional derivative of a given objective function. They, instead, rely on repeated evaluation of the objective function and obtain the search direction under nature-inspired heuristic guidelines. Though the derivative-free schemes are generally slower than derivative-based methods, they are much more effective for complicated objective functions and combinatorial problems as the methods do not require differentiable objective functions [1], [2].

So far, there have been a few researches on the use of combined GA and computational mechanics in structural design optimisation. These previous works may be divided into 3 main categories – the size, shape and topology design [3], [4].

In sizing optimisation, the topology and shape are held constant while specific dimensions of the design are modified. Examples include designs of plate thickness [2] and cross-sectional areas of truss and frame elements [5].

The shape optimisation maintains a constant topology while the shape is modified and design variables that produce optimum component shape are determined. The prime example is the shape optimisation by varying shape parameterisation and local curve fitting [6], [7]. It should be noted that the sizing optimisation typically occurs as a consequence of the shape optimisation process.

Meanwhile, the topology optimisation modifies topology of the design, allowing the creation of new boundaries. So far, the attemps to design optimal structures may be roughly divided into 3 main groups. The first involves the topology optimisation of discrete truss structures [8]. The second is the design of unit cell properties, orientation and porosity for performance optimisation of composite materials [9]. The last group concerns with the design optimization of continuum structures.

In this continuum topology design [4], if the maximum dimensional limits of a structure are specified, the volume space that contains the structure is known. As this space can be divided into small basic geometrical shapes, such as blocks or tetrahedrons, structures can be assembled from such basic shapes similar to a child's block buildings. Given prescribed design parameters, patterns of block arrangements that can superlatively perform certain objective functions can be found.

Thus, this procedure has the advantages that the topology of the structure may evolve freely and the absence of user bias as no a-priori knowledge about the topology is needed.

In this design process, the performances of structures must be evaluated with minimum human involvement if the structure may evolves efficiently. Numerical simulations fulfil these requirements very well and the finite element (FE) method has been employed in most previous cases, e.g. [4], [10], [11], [12].

It is this category of continuum structure optimisation that this paper fell into. Instead of stress analysis problems as in previous studies, the work involves a heat transfer test case and chooses the finite volume (FV) method for the calculation of the objective function. The advantages of this FV scheme are the

direct representation of conservative laws, straightforward physical interpretation, simple discretisation and the superior ability in handling strong non-linearities such as those found in CFD. With ongoing developments of a multidisciplinary unified code, multiphysics parameters and constraints should be readily available for future works.

2. Problem Descriptions

A 2D heat transfer problem with convective boundary is used as the example. Given a wall that is kept at a constant temperature, a limited space is available for attaching a solid protruding structure into the wall in order to facilitate the heat transfer into the surroundings. The design objective is to find the protruding configuration that allows highest heat loss from the wall.

In this feasibility investigation, the dimension of available space for the protruding structure is 1m × 1m with the thickness of 1 m. This structure-containing space is divided into 12 rectangles of equal size (Figure 1). Other parameters are prescribed as follows: the temperature of the wall = 100 °C, the ambient temperature = 0 °C, the thermal conductivity of the protruding solid k = 50 W/mK and the heat transfer coefficient from the wall and the protruding body into the surrounding air h = 20 W/m^{2}K. It is also assumed that the circulation of the air is so good that the ambient air temperature in close proximity to the wall and the protruding body remains constant at 0 °C.

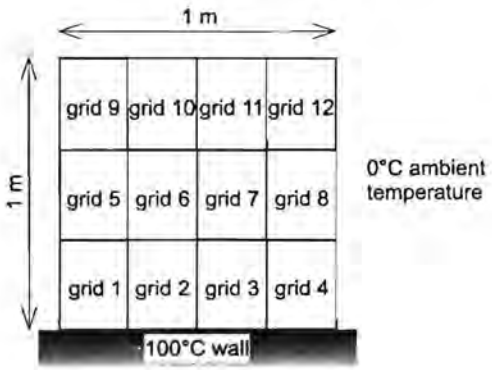

Figure 1 Problem descriptions

3. The Genetic Algorithm

The genetic algorithm is a derivative-free, population-based optimisation method that is inspired by concepts of natural selection and evolutionary processes [1], [13], [14].

The problem-specific knowledge is translated into the GA framework by the *encoding scheme*, which transforms points into bit string representations, called *chromosomes*. Each chromosome is associated with a *fitness value*, which is the parameter that is to be maximised by the algorithm.

In this study, patterns of solid block placement in the available space are encoded into 12-bit binary chromosomes. The block insertion on a grid, in the order illustrated in Figure 1, is represented by number '1' whilst number '0' signifies a void in the corresponding location. In addition, each configuration is assigned an index, obtained by converting the binary 'value' of the chromosome into a decimal number as shown in Figure 2.

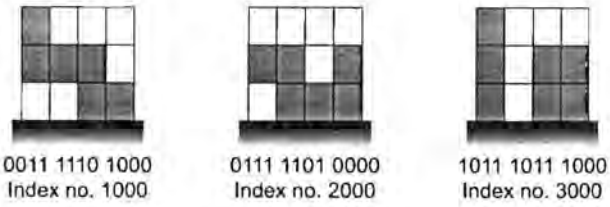

Figure 2 Examples of chromosome encoding and index. Shaded areas indicate filled grids while white grids are empty.

Instead of starting with a single initial point as in most derivative schemes, the GA stores a set of points as a *population*, or gene pool which is then evolved repeatedly toward a better overall value of the objective functions or *fitness*.

A group of randomly generated points in the solution phase space forms the first *generation*. Then, the population of the second generations are generated from the first generation members through *genetic operators*, namely selection, crossover, mutation and elitism, as shown in Figure 3.

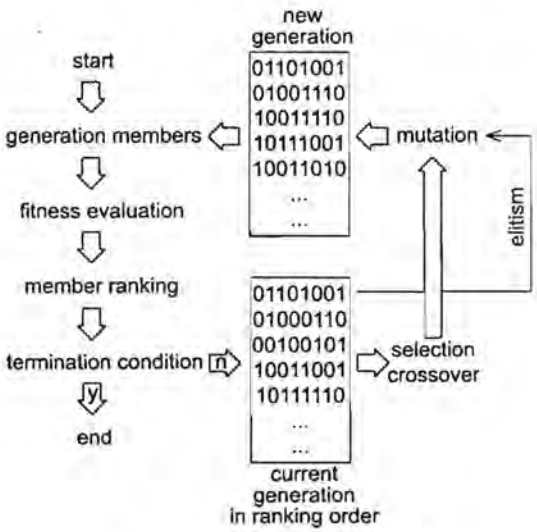

Figure 3 A GA evolution overview

The *selection* operation chooses which 'parent' chromosome pairs may reproduce the 'children' chromosomes for the next generation. The objective of a selection method is to encourage members with above-average fitness values to 'breed' rather than those with below-average fitness values. The most common selection scheme is the roulette wheel selection, in which members are selected with a selection probability p proportional to their fitness values:

$$p = f_i \Big/ \sum_{k=1}^{k=n} f_k \,, \tag{1}$$

where f_i is the fitness value of the ith member and n is the population size.

For each pair of selected parent chromosomes, two children chromosomes are generated through the *crossover* operator, which occurs at a probability equal to a crossover rate. The most basic crossover operator is the one-point crossover in which a crossover point is selected at random and parent chromosomes

are interchanged at this point, generating children chromosomes (Figure 4a). The effect of the crossover operation is analogous to the natural mating process in which parents pass segments of their chromosomes onto their children. That is, the crossover exploits current genetic potentials; some children are able to outperform their parents if they get good genetic traits from both parents.

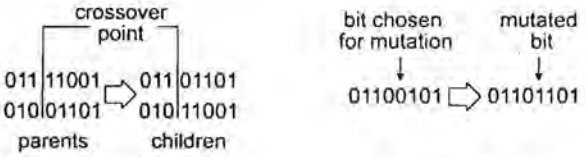

(a) one-point crossover (b) bit-flip mutation

Figure 4 Simple GA operations

These selection and crossover processes are repeated until the required number of the new generation is obtained. In addition, the *elitism* principle keeps a certain number of best chromosomes when a new population is generated. Elitism can increase performance of GA as it prevents the loss of good solutions.

However, the population may not contain all the necessary gene pool for the optimum solution. A *mutation* operator changes values of bits in the chromosomes (Figure 4b), introducing new routing solution randomly and therefore preventing stagnation at any local optima.

Hence, the second generation are produced. In this manner, new generations are repeatedly generated and evaluated as in Figure 3 until a stopping criterion is fulfilled, e.g. when the best ever chromosome remains unchanged for many generations or the number of generations reaches a prescribed value.

4. Fitness Evaluation by the Finite Volume Method

In this work, the configurations are rated according to their heat dissipating capability. The FV method models the temperature distribution in structures and the dissipated heat is calculated from the combined heat flux from the wall into the protruding structures and the surroundings. The higher the heat loss, the better the structure. For a configuration pair with equal values of dissipated heat, the structure that is made of less solid blocks is considered fitter.

4.1 Mathematical Models

The law of conservation of the energy in solids is employed as the governing equation. For a body in thermal equilibrium without internal heat sources, the equation takes the form:

$$\int_S q_i \, dS_i = 0 , \tag{2}$$

where the normal, outwards vector S_i presents the surface that bounds the body and q_i is the heat flux across the surface.

The Fourier's law of heat conduction for isotropic materials states that:

$$q_i = -k \frac{\partial T}{\partial x_i} , \tag{3}$$

where k is the thermal conductivity, T is the temperature and x_i is the position vector.

The boundary conditions for the example problem are the prescribed temperature at the wall – solid block interfaces and the surface convection everywhere else. The Newton's law of cooling expresses the overall effect of convection and the heat flux q^b leaving the solid into fluid per unit area as:

$$q^b = h(T^b - T^\infty) , \tag{4}$$

where h is the heat transfer coefficient, T^b is the temperature at the solid boundary and T^∞ is the ambient fluid temperature. Yet again, the assumption that the circulation of the fluid is very good such that the T^∞ remains constant is affirmed.

4.2 The Finite Volume Discretisation

The 2D mathematical model is discretised by a cell-centred FV technique for arbitrarily-shaped control volumes [15], [16]. Even though the problem can be modelled with simple rectangular control volumes [17], the more complicated scheme is used for future developments.

The spatial domain is discretised into a finite number of control volumes or cells. Figure 5 shows a typical cell P that is bounded by M faces m. The computational node P is placed at the centre of the cell. Moreover, there are non-computational boundary nodes that are introduced for the specification of boundary conditions.

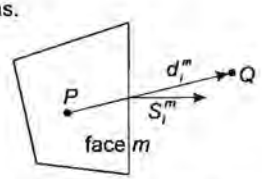

Figure 5 A control volume

The method assumes the second-order accurate spatial distribution. Gradients of a quantity ϕ at node P are calculated by ensuring a least square fit of ϕ through P and its neighbouring nodes.

The diffusion flux through the cell face m into a neighbouring node Q is approximated using the mid-point rule and the orthogonal correction approach as:

$$\int \frac{\partial T}{\partial x_i} dS_i^m \approx \left(\frac{T^Q - T^P}{d^m} + (\frac{\partial T}{\partial x_i})^m (\frac{S_i^m}{S^m} - \frac{d_i^m}{d^m}) \right) S^m . \tag{5}$$

For the convection boundary, the boundary temperature T^b is calculated by substituting equations (3) and (4) into (5):

$$T^b (h + \frac{k}{d^m}) \approx k \left(\frac{T^P}{d^m} + (\frac{\partial T}{\partial x_i})^m (\frac{S_i^m}{S^m} - \frac{d_i^m}{d^m}) \right) + h T^\infty . \tag{6}$$

Then, the temperature at a boundary cell face is incorporated into the cell equation by substituting T^Q by appropriate T^b in (5).

The equation for each control volume may be rearranged in the form:

$$a^P T^P - \sum_{m=1}^{M} a^Q T^Q = b , \tag{7}$$

where a^P and a^Q are respectively the discretised cell and its neighbour coefficients, b is the discretised source terms.

By assembling equation (7) of all control volumes, the system of algebraic equations is obtained with nodal temperatures as unknowns. The system is linearised, segregated and then iteratively 'solved' by the incomplete Cholesky conjugate gradient (ICCG) solver until a certain level of convergence is reached. The updated results are then used to update the non-linear terms; and the new system is 'solved'. This procedure is repeated until implicit solutions are achieved.

5. Results and Discussions

In order to better perceive the routing of GA, the heat transfer values of all 2^{12} or 4096 combinatorics are first calculated by FV prior to the GA procedure. In this preliminary study, a solid-filled grid is modelled with only one FV cell. The resulting heat loss data of all possible configurations are shown in Figure 6.

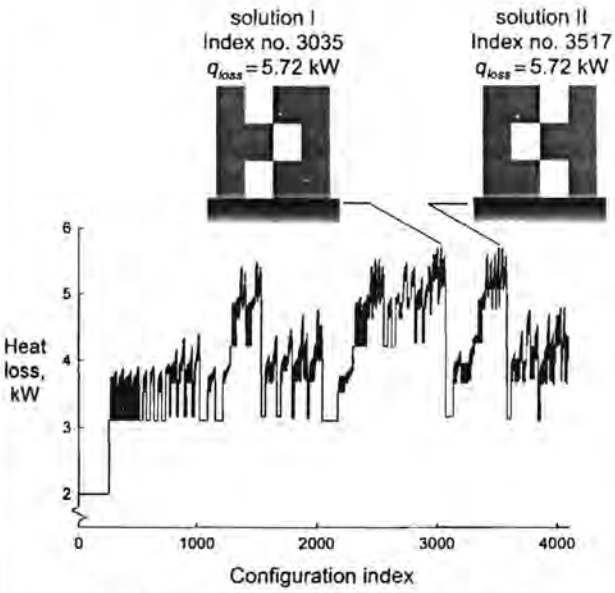

Figure 6 Heat loss from the wall for all configurations and the two optimum configurations

The total heat loss q_{loss} is calculated from the combined heat loss from the unattached wall segments and the heat flux across the wall-structure interface. The heat loss is influenced by the two main factors, the surface exposure and the temperature difference across the protruding structure-air boundaries.

At any unattached wall segments, the heat flux remains constants at 2 kW/m^2 as the boundary temperature T^b is constant. In the protruding structure, however, T^b is subject to the temperature distribution in the structure.

Figure 7 shows the wall-air and structure-air exposure areas of all configurations. When the exposure areas are compared with the heat loss values in Figure 6, it is clear that higher exposure area of the structures may not translate into high heat loss. At closer inspections, the key to high performances is the solid block topology which combines the exposure area with the structural connectivity that allows high boundary temperatures.

In many patterns, solid blocks are placed in positions that are not in physical contact with the rest of the structure. While these blocks mathematically increase the exposure areas, they are physically impossible and do not affect the performances.

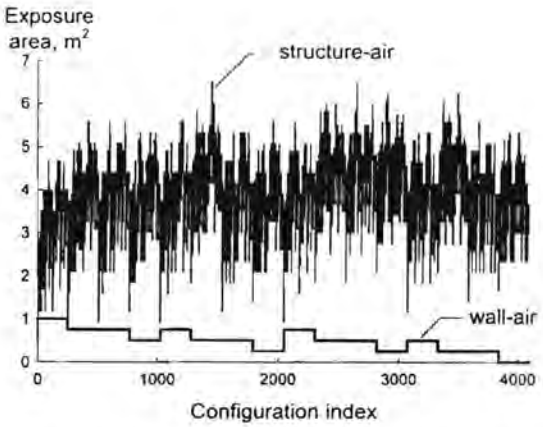

Figure 7 Surface exposure areas of all configurations

The extreme examples of the uncontact cases are trivial configurations 0 to 255 in which the protruding structures are not physically attached to the wall at all. All heat losses occur from the wall into the surroundings at the constant value of 2 kW.

Meanwhile, the configurations with the mathematically highest combined exposure area, consisting of 0.5 m^2 wall-air and 6.5 m^2 structure-air exposure areas, have bad connectivities that allow heat transfer in only 2 blocks as shown in Figure 8a.

Index no. 1445 q_{loss} = 4.21 kW | Index no. 1453 q_{loss} = 4.21 kW | Index no. 2650 q_{loss} = 4.21 kW | Index no. 2651 q_{loss} = 4.21 kW

(a) Configurations with maximum combined exposure areas

Index no. 1451 q_{loss} = 4.21 kW | Index no. 2395 q_{loss} = 4.84 kW | Index no. 2774 q_{loss} = 4.88 kW | Index no. 1461 q_{loss} = 4.90 kW

(b) Configurations with equal block and exposure areas

Figure 8 Example configurations for connectivity discussions. The lighter shaded area indicated unconnected blocks.

For another example, all patterns in Figure 8b are assembled from 7 blocks and have mathematical 0.5 m^2 wall-air and 6 m^2 structure-air exposure areas, shows different heat loss value.

This inclusion of unattached and discontinuous structures in the solution domain shows that this topology design approach imposes few constraints and completely ignores bias and normal

human reasoning processes, such as the inclusion of severely flawed solutions in the solution space. It is this total disregard of conventional knowledge that allows completely unexpected results to emerge in GA studies.

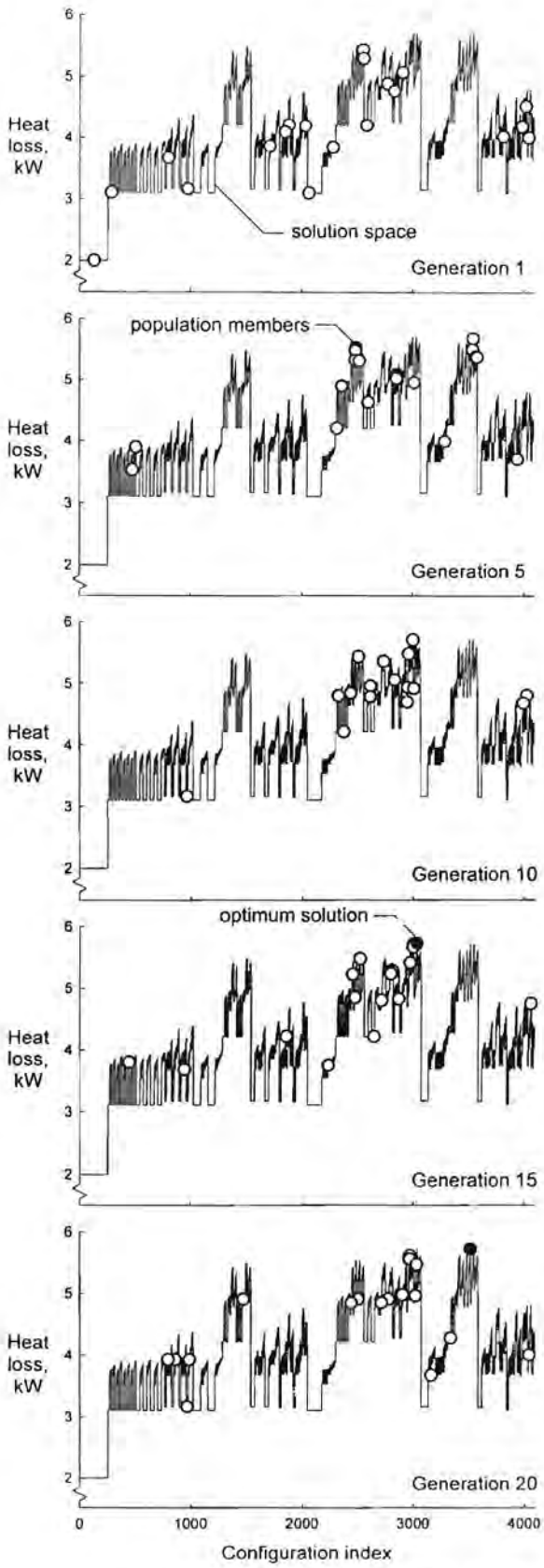

Figure 9 Population of generations 1, 5,10, 15 and 20.

By comparing the heat loss values of all combinatorics, two mirror-image optimum configurations are found. They have the heat loss value of 5.72 kW, the wall-air exposure area of 0.25 m^2

and the structure-air exposure area of 5.75 m^2 as displayed in Figure 6. Both solutions show the combination of high surface exposure and good grid connectivity in the structure.

It is clear that the heat loss curve in Figure 6 which is the objective function is not continuous. The phase space solution shows many abrupt changes and several spikes. Similar structures may yield drastically different fitness values. With no better means of configuration ordering, a differentiable relationship that adequately fits the heat loss functions is not judiciously obtainable. Moreover, with so many peaks, a derivative-based search routing is most likely trapped in local maxima. Thus, this problem calls for a derivative-free optimisation method, of which the GA is a popular option.

This study uses a basic GA based on the roulette wheel selection, one-point crossover and bit-flip mutation with elitism. The simple GA algorithm is not optimised and its control parameters are simply chosen as follows: total number of generation = 30, the population size in each generation = 20, number of elite chromosomes that survived to the next generation = 2, crossover rate = 1.0 and mutation rate = 0.1.

Figure 9 is the plot of the fitness function at every 5 generations with the population locations denoted by circles. In the first generation, the randomly generated members scatter all over the solution space. Within 5 generations, the population converges to various peaks and chromosomes at the lowest fitness range, especially in the cases that the structures are not in contact with the wall, are eliminated. Generally in any generation, the member locations mostly concentrate on high peaks. However, there are also a small number of members with a rather bad fitness values due to the mutation as exemplified in generation 10 and 20. It should be noted that even though no chromosome is presented in certain spikes in some later generations, a good deal of information is not really loss. Rather, chromosome segments are still mostly contained in the population gene pool and similar chromosomes may resurface later.

Figure 10 is the plot of the best, median and worst values of the population members across 30 generations. Due to the elitism, the best curve tends to monotonically increase with respect to generations. With mutation, the solution space may be explored in a random manner and the graph shows erratic behaviours as illustrated by the sharp drop of the worst member curve in generation 18.

The target optimum configuration I is obtained in generation 15 and the solution II in generation 19 as indicated in Figure 10. These optimum solutions are also marked in Figure 9 by filled circles as displayed in generation 15 and 20. The method shows the remarkable ability in avoiding local maxima stagnation. Moreover, several search routings simultaneously occur across generation such that both optimum results are obtained within 4 generations of each other.

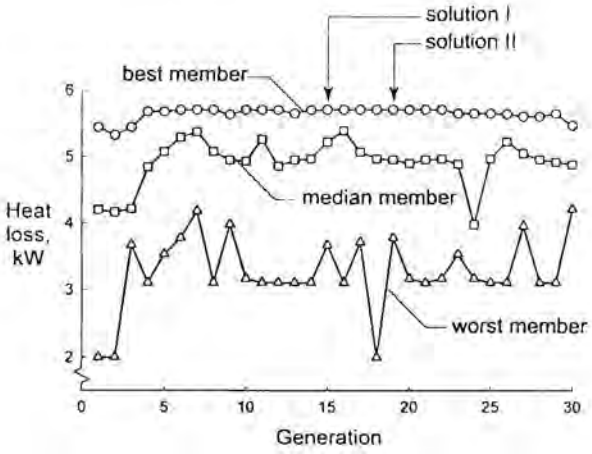

Figure 10 Performance of GA across generations

Convincingly, this optimisation process shows high potential for topology design of heat transfer problems. Similar previous works on stress analysis test cases has investigated more advanced GA procedures such as multicriterion and optimisation on much larger chromosomes [4], [10]. Therefore, the most straightforward future investigation involves such GA processes.

In addition, complex mathematical models that capitalize on FV strengths are needed. For instance, a conjugate heat transfer simulation will eliminate the assumption of constant ambient temperature and allows much more accurate fitness evaluation. More importantly, the grid dependency has not been addressed.

It is also noted that this design process is basically constrained by the shape and sizes of basic blocks. Thus, in the design of practical cases, integrated shape and sizing optimisation [12] are needed to further enhance the solutions.

6. Conclusions

In this paper, a preliminary topology design procedure using combined GA and FV method is examined. The concept and procedure of structural design by composition of basic unit shapes are presented. The design objective function is found to be discontinuous and unsuitable for derivative-based optimisation schemes. However, the derivative-free GA is able to find the optimum solutions without particular difficulties. The overall result of this feasibility study is promising enough that the procedure merits further investigation. Future developments will concentrate on the refinements of design concepts, GA and FV simulation before it is ready for practical applications.

7. Acknowledgement

This research work is supported by the Thailand Research Fund (TRF) for the Senior Scholar Prof. Pramote Dechaumphai and the New Researcher/Lecturer Endowment Fund, Chulalongkorn University. Numerous helps from Dr. Ratchatin Chanchareon are also highly appreciated.

References

[1] J.-S.R. Jang, C.-T. Sun, and E. Mizutani, "Neuro-Fuzzy and Soft Computing", Prentice-Hall, NJ, 1997.

[2] H. Sakamoto, S. Takada, J. Itoh, M. Miyazaki and A. Hijikata, "Investigation of a practical method of structural

optimization by genetic algorithms", JSME International Journal, Series A, vol. 44, no. 3, 2001, pp. 330-337.

[3] K. Lee, "Principles of CAD/CAM/CAE Systems", Addison-Wesley, 1999.

[4] M.J. Jakiela, C. Chapman, J. Duda, A. Adewuya and K. Saitou, "Continuum structural topology design with genetic algorithms", Computer Methods in Applied Mechanics and Engineering, vol. 186, 2000, pp. 339-356.

[5] K. Deb and D. Gulati, "Design of truss-structures for minimum weight using genetic algorithms", Finite Elements in Analysis and Design, vol 37, 2001, pp. 447-465.

[6] D. Quagliarella and A. Vicini, "Viscous single and multicomponent airfoil design with genetic algorithms", Finite Elements in Analysis and Design, vol 37, 2001, pp. 365-380.

[7] W. Annicchiarico and M. Cerrolaza, "Structural shape optimization 3D finite-element models based on genetic algorithms and geometric modeling"; Finite Elements in Analysis and Design, vol 37, 2001, pp. 403-415.

[8] N. Shankar and P. Hajela, "Heuristics driven strategies for near-optimal structural topology development", Artificial Intelligence and Structural Engineering, Civil-Comp Press, 1991, pp. 219-226.

[9] T. Matsuoka, S. Yamamoto and M. Takahara, "Prediction of structures and mechanical properties of composites using a genetic algorithm and finite element method", Journal of Materials Science, vol 36, 2001, pp. 27-33.

[10] K. Deb and T. Goel, " A hybrid multi-objective evolutionary approach to engineering shape design", Evolutionary Multi-Criterion Optimization, EMO 2001, LNCS 1993, Springer-Verlag, 2001, pp. 385-399.

[11] E. Sandgren, E. Jensen and J. Welton, "Topology design of structural components using genetic optimization methods", Proceedings of the Winter Annual Meeting of the American Society of Mechanical Engineers, 1990, pp. 31-43.

[12] F. Belblidia and E. Hinton, "Fully integrated design optimization of plate structures", Finite Elements in Analysis and Design, vol 38, 2002, pp. 227-244.

[13] T. Bäck, D.B. Fogel and Z. Michalewicz (ed.), "Evolutionary Computation 2 Advanced Algorithms and Operators", IOP Publishing Ltd, 2000.

[14] P. Chongstitvatana, "Evolutionary Computation: A Tutorial", http://www.cp.eng.chula.ac.th/faculty/pjw, 2000.

[15] H.G. Weller, G. Tabor, H. Jasak and C. Fureby, "A tensorial approach to computational continuum mechanics using object oriented techniques", Computers in Physics, vol. 12, no. 6, 1998, pp. 620-631.

[16] K. Maneeratana and A. Ivankovic, "Finite volume method for structural applications involving material and geometrical non-linearities", Proceedings of ECCM'99, Munich, Germany, 1999, no. 325.

[17] S.V. Patankar, "Numerical Heat Transfer and Fluid Flow", Hemisphere Publicating Corporation, 1980.

การประชุมวิชาการเครือข่ายวิศวกรรมเครื่องกลแห่งประเทศไทยครั้งที่ 16
14 – 16 ตุลาคม 2545 จังหวัดภูเก็ต

The Utilisation of Delaunay Triangulation in Finite Volume Modelling

Tanawut LERTSURAYUT and Kuntinee MANEERATANA
Department of Mechanical Engineering, Faculty of Engineering, Chulalongkorn University,
Phaya Thai Road, Pathum Wan, Bangkok 10330 Thailand
Phone 66(0)2218-6610 Fax 66(0)2252-2889 E-mail: kuntinee.m@chula.ac.th

Abstract

This paper concerns with the suitability study of meshes generated by the Delaunay triangulation for the finite volume modelling. In the unstructured cell-centred finite volume discretisation, the mesh-induced skewness error reduces the accuracy of surface integrals to the first order. In the mesh generation process, the Delaunay algorithm is controlled by two main parameters, α and β. It is found that the recommendation that $\alpha = 0.5$ and $\beta = 0.6$ for fine finite element mesh is also adequate to the finite volume requirements. The number of cells may be roughly controlled by varying the number of boundary points. The Laplacian smoothing technique satisfactorily reduces the distortion of triangular grids and is important for good grid quality. On the other hand, a new grid-adjusting scheme that further reduces the skewness error is unproductive as it may severely flatten and elongate the triangles such that the overall quality of control volumes is greatly reduced.

Keywords: Delaunay triangulation, Laplacian smoothing, finite volume method.

1. Introduction

This paper applies the Delaunay unstructured meshes, which has been used in finite element simulation [1], to finite volume models.

The development of the finite volume simulation has mainly focused on the handling of strong non-linearity and put less emphasis on the grid flexibility [2], [3]. Initially, the use of structured grid in finite volume modelling did not cause serious limitation. As the domain geometries of early problems tended to be relatively simple, the simulation could be performed effectively with body-fitted and curvilinear block structures. Modern applications, however, have such extremely complex domains that the unstructured grid is the only realistic answer.

Still, even in unstructured modelling, the finite volume models mostly use tetragons and hexahedrons with minimal triangles and tetrahedrons [4]. When the triangle and tetrahedral grids are concerned, the Delaunay triangulation or Delaunay-Voronoï method is a simple and popular grid construction method. The Delaunay-based method is well developed and tantalisingly close to become a black box grid generator [5].

Different discretising methods demand different attributes from the spatial discretisation. A grid that is well suited to a particular discretising scheme may not be in good standing in another. Thus, each grid generator must be examined for a particular discretisation scheme.

In this work, triangular meshes for the elliptic problems by an unstructured, cell-centred, finite volume method is considered. The heat conduction test cases are used to provide physical meanings.

2 Governing Equation

The law of conservation of the energy in solids is employed as the governing equation. With the Fourier's law of heat conduction for isotropic materials, the mathematical model takes the form:

$$\frac{d}{dt}\int_V \rho c T \, dV = \int_S k \frac{\partial T}{\partial x_i} \, dS_i + \int_V S \, dV \,, \tag{1}$$

where V is the volume of a body, bounded by the surface which is presented by the normal, outwards vector S_i, t is the time, ρ is the density, c is the specific heat, T is the temperature, k is the thermal conductivity, x_i is the position vector and S is the heat source.

For bodies in thermal equilibrium without internal heat source, equation (1) is reduced to the diffusion term:

$$\int_S k \frac{\partial T}{\partial x_i} \, dS_i = 0 \,. \tag{2}$$

3. The Finite Volume Discretisation

The 2D mathematical model is discretised by a cell-centred finite volume technique for unstructured meshes [6], [7]. The advantages of this scheme include the direct representation of conservative laws and straightforward physical interpretation.

3.1 Spatial Discretisation

The spatial domain is discretised into a finite number of triangular control volumes or cells as shown in Figure 1a. A typical cell P (Figure 1b), represented by the node P at the centre of the cell, is bounded by faces f. These faces are shared between P and adjacent cells Q^f. In addition, non-computational nodes at boundaries are introduced for the specification of boundary conditions.

3.2 Approximation of Diffusion Flux

The governing equation (2) can be exactly expressed for a cell P as:

$$\int_S k \frac{\partial T}{\partial x_i} \, dS_i = \sum_{f=1}^{3} \int_{S^f} k \frac{\partial T}{\partial x_i} \, dS_i = \sum_{f=1}^{3} k \left(\frac{\partial T}{\partial x_i}\right)^f S_i^f = 0 \,. \tag{3}$$

The method assumes the second-order accurate spatial distribution for any variables. That is, the truncation error ε is

proportional to δx^2, where δx is the cell size. The value of a quantity ϕ at cell face f between P and Q^f is calculated by:

$$\phi^f = \frac{\phi^P + \phi^{Q^f}}{2} + \frac{g_i^P (r_i^f - r_i^P) + g_i^{Q^f} (r_i^f - r_i^{Q^f})}{2}, \quad (4)$$

where g_i is the gradient of ϕ, r_i is the position vector and the superscript denotes the location of the property. The gradient vector g_i at a cell P is calculated by ensuring a least square fit of ϕ through P and neighbouring nodes Q^f as:

$$\left(\sum_{f=1}^{3} d_i^f d_i^f\right) g_i^P = \sum_{f=1}^{3} (\phi^P + \phi^{Q^f}) d_j^f, \quad (5)$$

where $d_i^f = r_i^{Q^f} - r_i^P$ is the distance vector between P and Q^f.

Thus, the diffusion flux through the cell face f into a neighbouring node Q^f can be approximated as:

$$k(\frac{\partial T}{\partial x_i})S_i^f = k\frac{S^f}{d^f}(T^{Q^f} - T^P) + k(\frac{\partial T}{\partial x_i})^f k_i^f, \quad (6)$$

where the correction vector $k_i^f = S_i^f - \delta_i^f$ as shown in Figure 1b. In the orthogonal correction approach, $\delta_i^f = S^f d_i^f / d^f$.

Therefore, the diffusion term is approximated by:

$$k(\frac{\partial T}{\partial x_i})S_i^f \approx k\frac{S^f}{d^f}(T^{Q^f} - T^P) + k(\frac{\partial T}{\partial x_i})^f (S_i^f - \frac{S^f}{d^f} d_i^f). \quad (7)$$

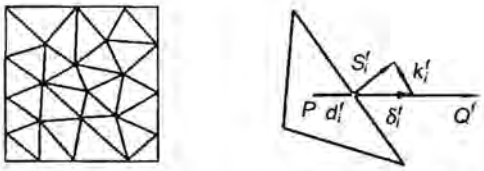

(a) unstructured grid (b) a typical control volume

Figure 1 Unstructured finite volume cells

3.3 Algorithms

The equation for each control volume may be rearranged in the form:

$$\left(\sum_{f=1}^{3} k\frac{S^f}{d^f}\right)T^P - \sum_{f=1}^{3}\left(k\frac{S^f}{d^f}T^{Q^f}\right) = \sum_{f=1}^{3}\left(k(\frac{\partial T}{\partial x_i})^f (S_i^f - \frac{S^f}{d^f} d_i^f)\right). \quad (8)$$

By assembling equations (8) of all control volumes, the system of algebraic equations $[A][T] = [b]$ is obtained with nodal temperatures $[T]$ as unknowns. The system is linearised, segregated and then iteratively 'solved' by the incomplete Cholesky conjugate gradient (ICCG) solver until a certain level of convergence is reached. The updated results are then used to update the non-linear terms; and the new system is 'solved'. This procedure is repeated until implicit solutions are obtained.

3.4 The Skewness Error

The skewness error, which reduces the accuracy of face integrals to the first order, is mesh-induced. Figure 2 shows a typical mesh distortion that causes the skewness error when the distance vector d_i^f does not cross a face at its centre f, but at point f^* instead.

The skewness error in the diffusion term on a face f may be obtained using the second-order distribution (4) as:

$$E_s^f = k\left((\frac{\partial T}{\partial x_i})^f - (\frac{\partial T}{\partial x_i})^{f^*}\right)S_i^f \approx k\frac{\partial}{\partial x_j}(\frac{\partial T}{\partial x_i})^f m_j^f S_i^f, \quad (9)$$

where $m_i^f = r_i^f - r_i^{f^*}$. Thus, the error on a face f depends on the second spatial derivative of T, vector m_i^f and surface vector S_i^f.

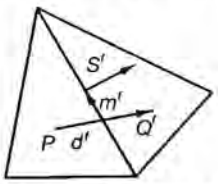

Figure 2 Skewness error on a face f.

That is, the size of vector m_i^f is a skewness-indicating parameter. In order to compare the indicator values from cells of different sizes, the normalised parameter m^f/d^f is used to quantify the skewness of a face f. The lower the m^f/d^f, the less skew the face. It is noted that a similar analysis for convection term requires m^f to be less than d^f [8].

3.5 Mesh Quality Assessment

Thus, it can be argued that the ideal shape of control volumes is equilateral triangle. Meshes entirely composed of such triangles have the best combination of no skewness errors and similar cell size δx in addition to the more accurate approximation of constant weight function across the cells in the volume integral (1).

The generated mesh quality may be assessed by comparing the statistical distribution of a certain indicator compared to that of the optimal mesh [5]. This work uses the value of maximum angles θ_{max} in any elements as the quality indicator. In an optimum grid, $\theta_{max} = 60°$.

4. Grid Generation

The section concerns with the triangular mesh generation by the Delaunay triangulation [1], [5]. The shape and size of resulting triangles are normally improved by the Laplacian smoothing technique. In addition, a new iterative grid-adjusting scheme, which is customised to reduce the skewness error in the employed finite volume discretisation, is described.

4.1 Delaunay Triangulation

The 2D Delaunay algorithm may be divided into 2 steps. First, the boundary triangles are generated by connecting boundary points on domain boundaries.

1. Insert I boundary points on the domain boundary in the counter-clockwise direction as shown in Figure 3a.
2. For a point i, the point distribution function $dp_i = (L_1 + L_2)/2$ with dimensional symbols shown in Figure 3a.
3. Generate the boundary triangulation as described in [1] and displayed in Figure 3b.

As the boundary triangles are very coarse, the mesh is refined by repeated refinement sweeps. This point insertion is controlled by two parameters, α and β. The point insertion procedures for any triangles are:

1. Calculate the centroid c of the triangle and the average distribution function of the triangle $dp_c = (dp_1 + dp_2 + dp_3)/3$ as described in Figure 3b.
2. The α criterion requires all distances $S_i > (\alpha \times dp_c)$ as defined in Figure 3c.

3. The β criterion requires all distances $d_i > (\beta \times dp_c)$ as shown in Figure 3d.

4. A new point is inserted at c and new triangles are generated as shown in Figure 3e if both α and β criteria are satisfied

Thus, the Delaunay triangulation of a given domain is influenced by 3 parameters, the number of boundary points, α and β. In practice, the values of α and β are between 0.0 – 1.0.

The α controls point density by changing the allowable shape of the formed triangle while the β promotes the triangles regularity by disallowing points in the same sweep when points are too close. Thus, if α and β are held constant, the overall shape and quality of the resulting triangles do not change significantly.

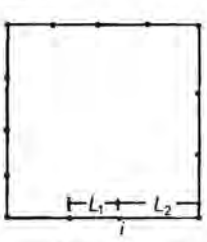

(a) boundary point insertion

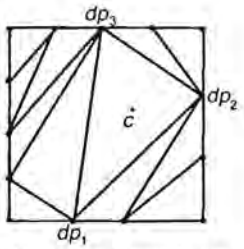

(b) boundary triangulation

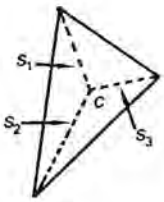

(c) α-controlled point insertion

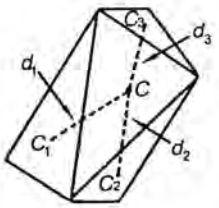

(d) β-controlled point insertion

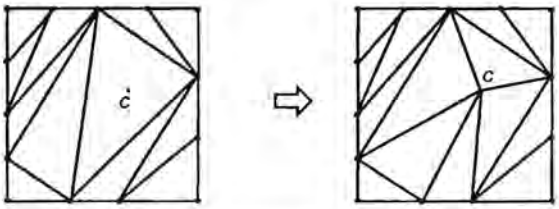

(e) point insertion and resulting new triangles

Figure 3 Delaunay grid generation procedure

4.2 Laplacian Smoothing

The Laplacian smoothing is a standard algorithm in the Delaunay grid generation. It improves the overall quality of the mesh by point repositioning.

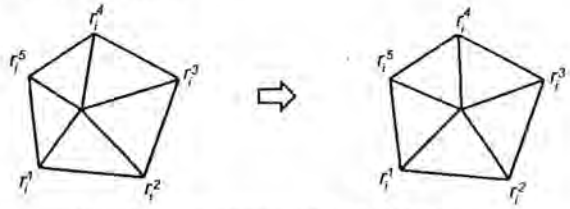

Figure 4 Laplacian smoothing technique

For each point, an enclosing polygon may be created by combining triangles that have the point as vertices as shown in Figure 4. The scheme moves the point under consideration to the centroid of the polygon. Such Laplacian point relocation is implemented for all interior points throughout the entire mesh.

4.3 Skewness Correction Smoothing

In addition to the Laplacian technique, a new iterative skewness correction procedure for finite volume discretisation is presented. The algorithm iteratively corrects the skewness by moving the point to minimise overall skewness of adjacent triangles in the enclosing polygon for every point v_i as shown in Figure 5:

$$\min\left(\sum_{k=1}^{K} l^k - \sum_{k=1}^{K}(m^k + n^k)\right). \tag{10}$$

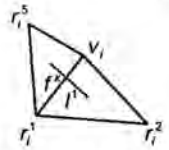

(a) distance l^k between nodes of adjacent triangles

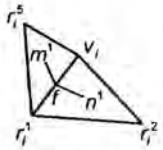

(b) distances m^k and n^k from the nodes to face f

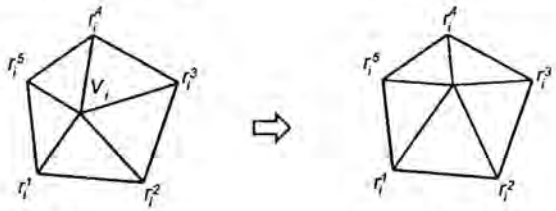

(c) original polygon (d) adjusted polygon

Figure 5 Skewness correction smoothing

5. Results and Discussions

In the evaluation of Delaunay grids for finite volume simulation, a square domain with the area of 1 m^2 is considered. For numerical modelling, two test problems on the generated meshes are studied. The problem definitions and analytical results of test case 1 and 2 are shown in Figure 6 and Figure 7, respectively.

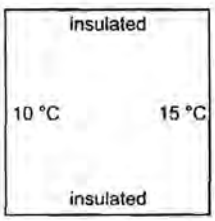

(a) problem definition

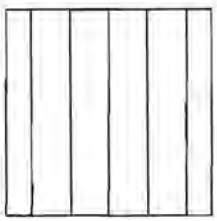

(b) analytical result

Figure 6 Problem definition and analytical result of test case 1

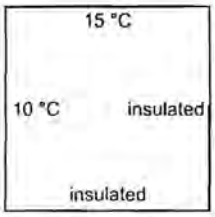

(a) problem definition

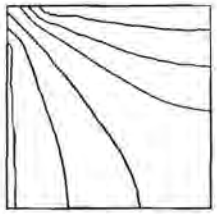

(b) analytical result

Figure 7 Problem definition and analytical result of test case 2

In the first part of the study, the domain boundary is divided into 20 intervals of equal size while the values of α and β vary

between 0.3 and 0.8 with 0.1 increments. The Laplacian smoothing is employed as in standard finite element grid generation.

Figure 8 shows selected grids and their overall quality. Typically, the grids with low values of α and β are finer while those with high α and β are coarser.

When the whole range of meshes is considered, it is found that when the value of α is held constant and the value of β varies, the resulting mesh alters when the α and β values are not very dissimilar. But when the values differ significantly, or roughly about 0.3, the resulting mesh stops changing. This is also true when β is constant and α changes.

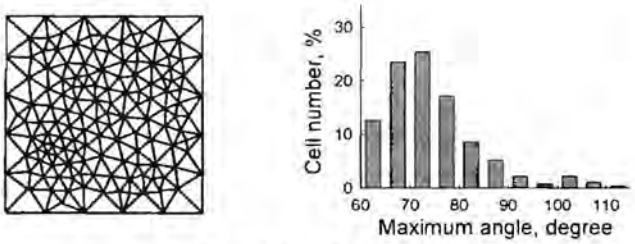

(a) $\alpha = 0.3$ and $\beta = 0.3$

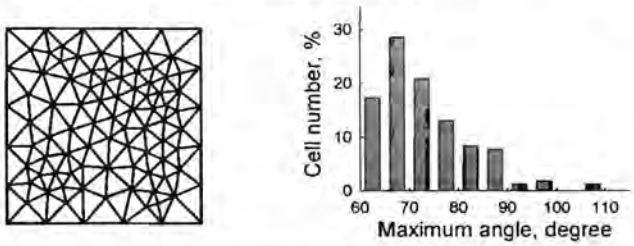

(b) $\alpha = 0.4$ and $\beta = 0.4$

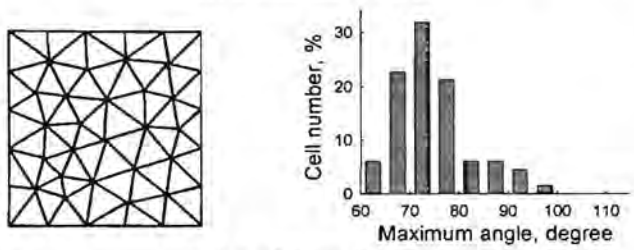

(c) $\alpha = 0.6$ and $\beta = 0.6$

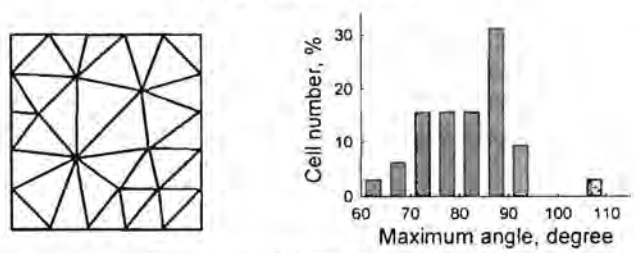

(d) $\alpha = 0.8$ and $\beta = 0.8$

Figure 8 Examples of grids and overall quality at various α and β.

This is due to the fact that the mesh refinement only functions when both α and β criteria are satisfied. When α and β values differ greatly, the point insertions tend not to occur and the grid stays the same. Therefore, it is unnecessary to consider α and β combinations when values α and β differ significantly.

The values of maximum, average and standard deviation of the overall quality and skewness indicators of the whole range are shown in Figure 9 and Figure 10 respectively. The maximum numerical errors ε_{max} of test cases 1 and 2 are respectively displayed in Figure 11a and Figure 12a. This absolute maximum error comparison is not particular useful as $\varepsilon \propto \delta x^2$. Thus, the ratios of maximum error over average cell size square are also presented. It should be noted that for the analytical solution of test case 1, $\partial^2 T/\partial x^2 = 0$. Thus, the skewness error on the accuracy is effectively eliminated as analysed in (9).

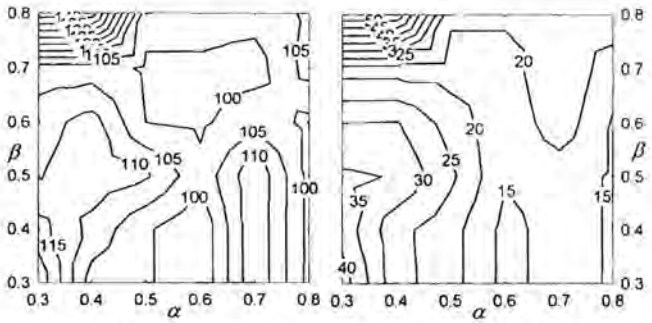

(a) maximum θ_{max}, degree (a) maximum m^l/d^l, %

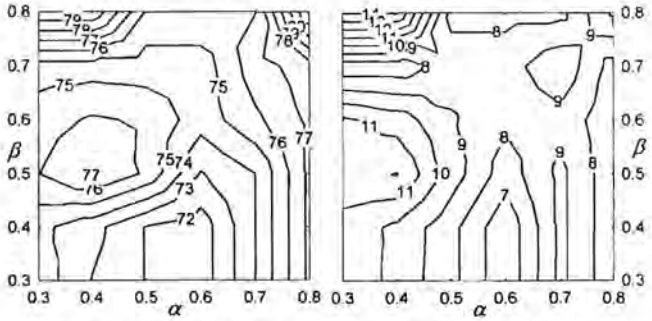

(b) average θ_{max}, degree (b) average m^l/d^l, %

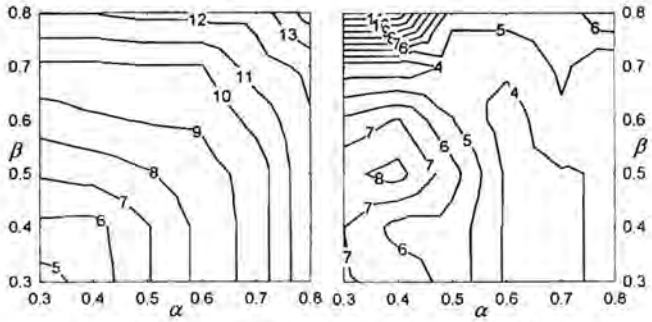

(c) S.D. θ_{max}, degree (c) S.D. m^l/d^l, %

Figure 9 Overall indicator Figure 10 Skewness indicator

In the finite element grid generation, the values of $\alpha = 0.5$ and $\beta = 0.6$ are recommended [9]. These recommendations are found to lie in the regions of very good grid quality and low skewness (Figure 9 and Figure 10) as well as that of accurate numerical results (Figure 11 and Figure 12). Even though the results at this grid may not be the best, the changes of domain and boundary point numbers also influenced the grid quality and, hence, numerical results. The best combination of α and β for a particular problem does not necessary yield best results in others. Thus for general utilisation it is futile to use the best α and β combination for this example problem. It is better to choose α and β combination that is certain to always provide satisfactory grid quality instead. Hence, it is suggested that the

recommended α and β for finite element grids are also acceptable to the finite volume requirements.

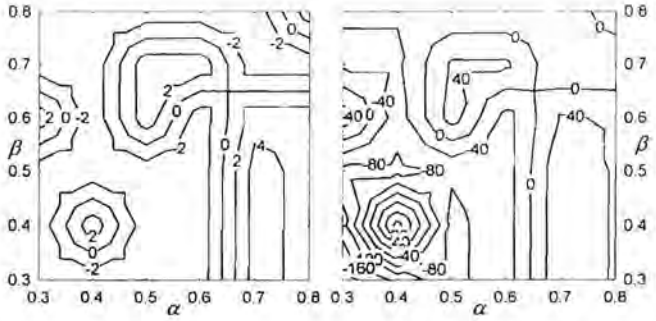

(a) ε_{max}, 10^{-5} (b) $\varepsilon/\delta x^2$, $10^{-5}/m^2$

Figure 11 Maximum errors of test case 1

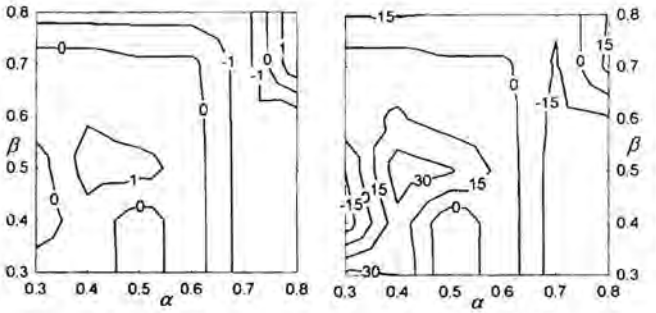

(a) ε_{max}, % (b) $\varepsilon/\delta x^2$, $\%/m^2$

Figure 12 Maximum errors of test case 2

As a rule, the Laplacian smoothing is used in the finite element grid generation to improve the overall quality of the grid. As this smoothing technique does not aim at reducing the skewness error, which is distinctive to the finite element discretisation as previously described, a skewness correction scheme is proposed.

Figure 13 shows a typical example of the smoothing effects on the grid quality and the numerical results while Figure 14 shows the overall numerical results of test case 2 without the Laplacian smoothing.

It is found that the Laplacian smoothing technique significantly improves the overall grid quality, reduces the skewness as well as numerical errors. In short, while the Laplacian smoothing cannot totally eliminate the skewness error, it can sufficiently reduce the distortion of triangular grids such that numerical results show good agreements with analytical solutions.

On the other hand, a new grid-adjusting scheme that further reduces the skewness error is unproductive as it may severely flatten and elongate the triangles as shown in Figure 13c. The overall skewness of the grid may be lower than that of the grid without the correction but the overall quality of control volumes is greatly reduced such that the numerical results are much less accurate. Occasionally, the grid quality is so bad that the numerical computation diverges. It is noted that the grids with $I=16$ is presented in Figure 13 instead of $I=20$ as the numerical simulations for the mesh with skewness correction diverges.

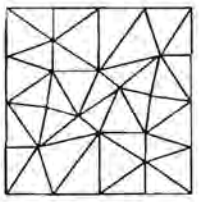

cell no.: 38
θ_{max}: max 106°
avg 83.6°
S.D. 13.6°
m^l/d^l: max 0.277
avg 0.133
S.D. 0.056

errors in test case
1: max 0.000%
avg 0.000%
S.D. 0.000%
2: max 0.498%
avg 0.014%
S.D. 0.193%

(a) without Laplacian smoothing

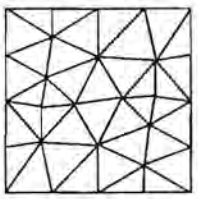

cell no.: 38
θ_{max}: max 99.3°
avg 79.4°
S.D. 12.9°
m^l/d^l: max 0.228
avg 0.098
S.D. 0.056

errors in test case
1: max 0.000%
avg 0.000%
S.D. 0.000%
2: max 0.445%
avg 0.013%
S.D. 0.139%

(b) with Laplacian smoothing (normal procedure)

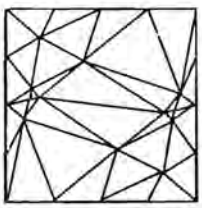

cell no.: 38
θ_{max}: max 156°
avg 93.8°
S.D. 15.2°
m^l/d^l: max 0.220
avg 0.092
S.D. 0.051

errors in test case
1: max 0.000%
avg 0.000%
S.D. 0.000%
2: max -0.659%
avg 0.024%
S.D. 0.289%

(c) with Laplacian smoothing and skewness correction

Figure 13 Effects of smoothing and skewness correction when $\alpha = 0.5$ and $\beta = 0.6$

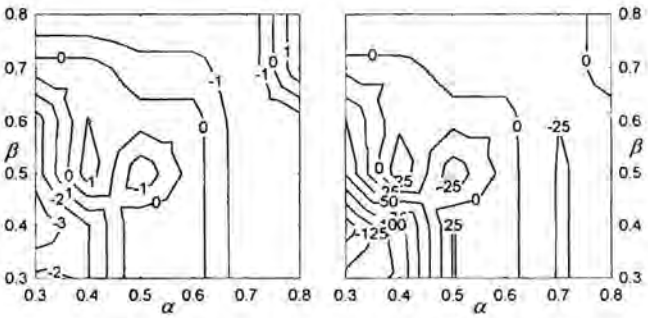

(a) ε_{max}, % (b) $\varepsilon/\delta x^2$, $\%/m^2$

Figure 14 Maximum errors of test case 2 without Laplacian scheme

Apart from α and β, the other parameter is the number of boundary points I. When the α and β are held fixed and the value of I varies, it is found that the overall shape of the triangles does not drastically change as exemplified in Figure 15. Thus, if the number of control volumes in a mesh is approximately prescribed by the user, the number of boundary points may be adjusted to obtain a mesh with roughly requested number of cells.

The procedure previously suggested for Delaunay grid generation is for general uses. It may provide reasonably good meshes in most situations, but cannot normally achieve the best grid for a given domain. If the rough number of control volumes in a given domain is prescribed by the user, the best α and β combination, while may be reasonably expected to be close to the recommended values, is unique. The only means to obtain

the optimum grid with the best quality is by optimisation with α, β and boundary point numbers l as parameters.

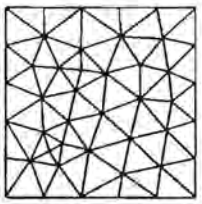

cell no.: 70		errors in test case	
θ_{max}:	max 100°	1: max	0.000%
	avg 75.9°	avg	0.000%
	S.D. 9.07°	S.D.	0.000%
m^l/d^l:	max 0.229	2: max	0.422%
	avg 0.091	avg	0.007%
	S.D. 0.051	S.D.	0.089%

(a) boundary point number $l = 20$

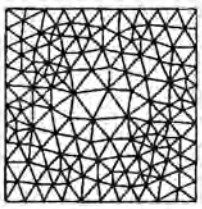

cell no.: 266		errors in test case	
θ_{max}:	max 105°	1: max	0.000%
	avg 74.5°	avg	0.000%
	S.D. 4.57°	S.D.	0.000%
m^l/d^l:	max 0.276	2: max	0.391%
	avg 0.096	avg	0.001%
	S.D. 0.062	S.D.	0.043%

(b) boundary point number $l = 40$

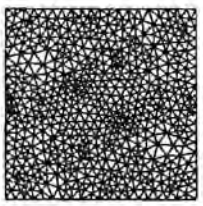

cell no.: 1182		errors in test case	
θ_{max}:	max 109°	1: max	0.000%
	avg 71.6°	avg	0.000%
	S.D. 2.08°	S.D.	0.000%
m^l/d^l:	max 0.263	2: max	0.341%
	avg 0.075	avg	0.000%
	S.D. 0.052	S.D.	0.020%

(c) boundary point number $l = 80$

Figure 15 Effects of boundary point numbers when $\alpha = 0.5$ and $\beta = 0.6$

In some way, this yearning for the 'best' grid is essentially wasted. The ultimate objective of computational mechanics is to obtain sufficiently accurate results that may be used. It is much more productive to concentrate on the result accuracy than on the grid quality.

From the error analysis and the numerical result of this study, the influences of skewness errors depends on $\partial^2 T/\partial x^2$ such that the truncation error is increased to be proportional to δx. Therefore, instead of trying to generate the optimum mesh with control volumes of regular shape and low skewness, more accurate results can be obtained using the adaptive grid [10]. In this algorithm, the cells with high gradient of solution gradients are refined while those in less crucial regions are coarsened. That is, the high accuracy may be simply achieved by reducing cell sizes and the skewness issue is alleviated.

6. Conclusions

The unstructured grids generated by Delaunay triangulation are evaluated for finite volume modelling. The cell-centred finite volume discretisation for unstructured triangular meshes are described. Grids requirements are explained and the overall quality and skewness indicators are chosen. The overall triangle quality is indicated by the largest angle while the ratio of skewness vector over the distance vector describes the skewness. Then, the procedure of Delaunay grid generation is simply illustrated.

A simple square domain is used as the example. It is found that the Delaunay parameters α and β should be similar. The recommended α and β in finite element grid are acceptable for the finite volume requirements. The Laplacian smoothing efficiently reduces the distortion while the skewness correction scheme is unsuccessful. The accuracy of the numerical simulations depends on both the quality and the size of the control volumes.

Therefore, in the absence of grid optimisation or, better yet, the adaptive grid algorithm, it is suggested that the recommended values of $\alpha = 0.5$ and $\beta = 0.6$ are used. The Laplacian smoothing is then employed to improve overall quality. The numbers of control volumes in the grids adjusted by changing the number l of boundary points.

7. Acknowledgement

This research is supported by the Thailand Research Fund (TRF) for the Senior Scholar Prof. Pramote Dechaumphai. Special thanks are due to Prof. Pramote Dechaumphai and Mr Sutthisak Phongthanapanich.

References

[1] S. Phongthanapanich and P. Dechaumphai, 2001, "Unstructured mesh generation with Delaynay triangulation and mesh refinement with local spacing control", Proceedings of ME-NETT15, Srinakharinwirot University, 2001, pp. CM 85-89.

[2] S.V. Patankar, "Numerical Heat Transfer and Fluid Flow", Hemisphere Publicating Corporation, 1980.

[3] J.H. Ferziger and M. Peric, "Computational Methods for Fluid Dynamics", 2nd edition, Springer-Verlag, 1999.

[4] Nabla Ltd., "FOAM C++ Library", http://www.nabla.co.uk.

[5] J.F. Thompson, B.K. Soni and N.P. Weatherill, "Handbook of Grid Generation", CRC Press, 1999.

[6] H.G. Weller, G. Tabor, H. Jasak and C. Fureby, "A tensorial approach to computational continuum mechanics using object oriented techniques", Computers in Physics, vol. 12, no. 6, 1998, pp. 620-631.

[7] K. Maneeratana and A. Ivankovic, "Finite volume method for structural applications involving material and geometrical non-linearities", Proceedings of ECCM'99, Munich, Germany, 1999, no. 325.

[8] H. Jasak, "Error analysis and Estimation for the finite volume method with applications to fluid flows", PhD Thesis, Imperial College of Science, Technology and Medicine, University of London, 1996.

[9] B.K. Karamete, T. Tokdemir and M. Ger, "Unstructured grid generation and a simple triangulation algorithm for arbitrary 2-D geometries using object oriented programming", International Journal for Numerical Methods in Engineering, vol. 40, 1997, pp. 251-268.

[10] P. Dechaumphai, T. Sricharoenchai and S. Phongthanapanich, "Evaluation of adaptive Delaunay triangulation for crack propagation problems", Proceedings of ETM 2002, Bali, 2002, pp. 1-12.